**How much does traffic contribute to benzene and PAH air pollution? Results from a high-resolution North American air quality model centered on Toronto, Canada.**

**SUPPLEMENT**

**Contents**

### I.        Model process representation and setup

Regional air-quality models are the means by which the impact of a single emissions source on pollutant concentrations may be evaluated. These models solve the comprehensive partial differential equations describing the rates of change of atmospheric chemical tracers in three dimensions, through the use of operator splitting and specialized solvers for specific atmospheric processes (Jacobson *et al*, 2005). These models were originally developed in response to the need to determine the sources of acidifying precipitation (e.g., Chang *et al*, 1987), and have been expanded and modified over the subsequent years for an increasing number of atmospheric applications. Regional air-quality models were first applied to the problem of PAH predictions for a European continental domain (Aulinger *et al*, 2007) and the region surrounding the city of Rome (Gariazzo *et al*, 2007). Global PAH sources and resulting spatial and temporal distribution have been examined using a global model (Friedman *et al*, 2012; Thackray *et al*, 2015). North American PAH and benzene emissions and reaction chemistry have been studied using both ``off-line" (Galarneau *et al*, 2014; Stroud *et al*, 2016; Zhang *et al* (2016,2017) and ``on-line" regional air-quality models (Whaley *et al*, 2018). Off-line models make use of meteorological output from a weather forecast model to drive the advection and diffusion portions of the regional air-quality model, while on-line models are a more recent development, in which the chemical and meteorological processes are incorporated into a single modelling framework in order to more efficiently predict chemical concentrations and avoid errors associated with interpolation between weather forecast and regional air-quality model grids (e.g. Grell *et al*, 2005, and Makar *et al*, 2015a,b for a detailed discussion of on-line models and an intercomparison of their results).

We refer the reader to Whaley *et al.* (2018) for further detail on GEM-MACH-PAH model development and setup. Here we briefly summarize the model PAH and benzene processes, as described in more detail in that work, as well as the model run setup for the current mobile source contribution study

***Process Representation:***
The processes governing PAH and benzene concentrations within the model include gas-particle partitioning (for PAHs; benzene exists only in the gas-phase), advection, vertical diffusion, OH radical gas-phase oxidation, $O_3$ particle-phase oxidation for BaP, cloud processing, and dry and wet deposition. GEM-MACH includes 8 speciated components to total particulate matter; sulphate, nitrate, ammonium, elemental carbon, primary organic matter, secondary organic matter, crustal material and sea salt. This scheme includes both the total OC (total organic carbon) and EC (elemental carbon) as carbon pools; the GEM-MACH model explicitly speciates these OC and EC components of particulate matter, further subdividing OC into primary and secondary components. In GEM-MACH-PAH, 7 PAHs (listed in the main text) are also added to the particle speciation.

PAHs and benzene are emitted in the gas-phase, and rapid repartitioning of the PAHs between the gas and particle phases occurs after emissions. Emissions from large stack industrial sources are distributed in the vertical using plume rise equations, while emissions from smaller sources are amalgamated into net surface source emissions within each grid cell, and are added to the model as a flux boundary condition on the diffusion equation within the vertical diffusion solver. PAH gas-particle partitioning is carried out using the Dachs-Eisenreich (2000) approach that was

improved relative to previous work by Galarneau *et al* (2014) by adjusting partitioning parameters according to available phase-separated measurements.

Our GEM-MACH-PAH simulations make use of the model's operational forecast configuration, with a two-bin (fine and coarse) sectional approach for particulate species. Particle microphysics processes requiring higher particle size resolution, such as coagulation, temporarily subdivide these bins for more accurate process representation. Advection of all tracers within GEM-MACH is carried out using a semi-Lagrangian approach employing a cubic Lagrange interpolant with a subsequent global mass conservation correction. Tracer vertical diffusion employs K-theory diffusivities calculated by the GEM meteorological model, and a single-step backward difference numerical solver. Particulate BaP undergoes a reaction with $O_3$ via the Kwamena (2004) scheme, and all gaseous PAHs and benzene undergo reaction with OH, with rate constants as presented in Galarneau *et al* (2014) and SAPRC-07 toxics (Carter, 2010; Hutzell *et al*, 2012), respectively.

Particulate PAHs undergo no additional particulate surface reactions aside from the benzo[a]pyrene surface reaction with ozone. Aside from partitioning with the gas-phase, particulate PAH mass may be reduced through particulate deposition, which is a function of the size of the particles within which the PAHs reside. Gas-phase PAH deposition follows the approach taken for other gases in GEM-MACH (see the SI of Makar *et al.,* 2018); a multiple resistance, temperature-dependent "big-leaf" approach, employing parameters based on Henry's law constants and water solubility. Gaseous PAHs and benzene may also be scavenged by cloud water and rain via Henry's Law and by snow surface adsorption (Franz and Eisenreich, 1998). Further details and references for GEM-MACH-PAH process representation may be found within Whaley *et al.* (2018).

### *Model Setup: Nesting Configuration and Forecast Cycling Procedures*
The model cycling procedure mimics an operational nested forecasting system, in which a continental 10 km simulation provides continuity between forecast cycles. In order to prevent chaotic drift from the observed meteorology, the 10 km resolution simulation's meteorology was re-initialized from *a priori* GEM forecasts that made use of data-assimilated analysis fields from the Canadian Meteorological Centre, at each forecast cycle. The continuity between air-quality forecast cycles was thus maintained at the 10 km simulation level (see Figure S.1); the nested 2.5 km domain provides a high-resolution refinement to the 10 km resolution forecast for each day. Figure S1 also shows the linkage between forecast cycles. Three successive forecast cycles are shown (Days 1, 2 and 3; Figure S.1). Red arrows indicate the transfer of model initial conditions between the 10km North American domain GEM-MACH simulation, the current cycle's 2.5 km refinement, and the subsequent cycle's 10 km simulation. Blue arrows indicate the flow of information to stitch together the final 2.5 km forecasts.
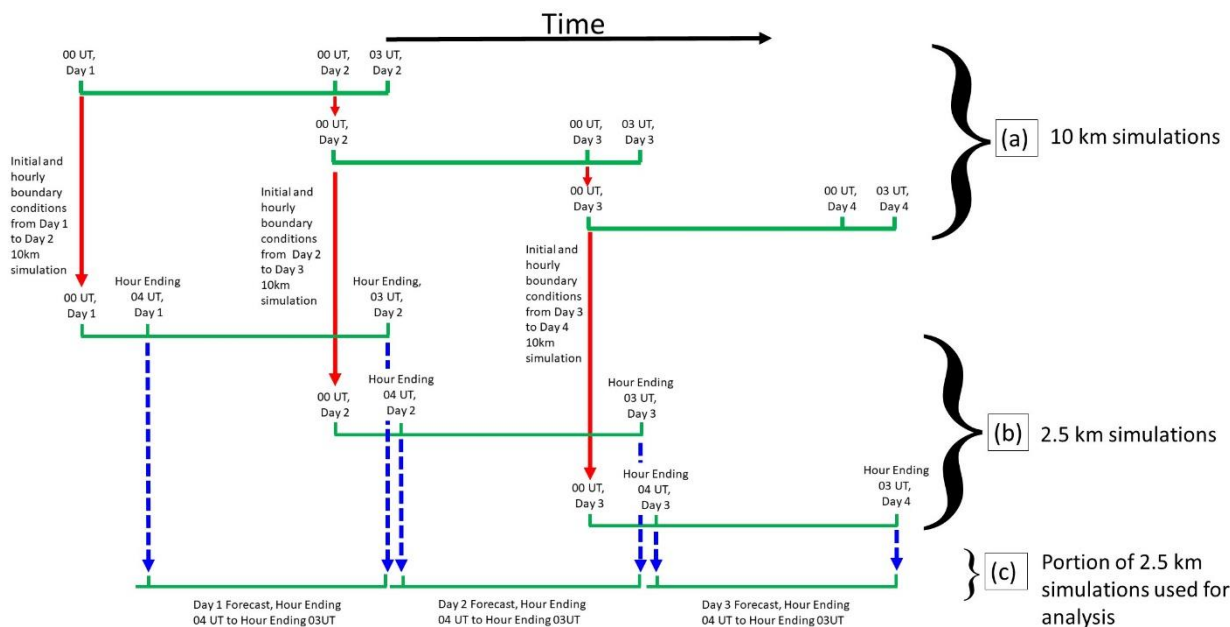
**Figure S.1.** Timeline of forecast cycle for GEM-MACH-PAH. The horizontal direction in this figure is the time axis. Green bars represent the timeline of a single forecast cycle at a given model resolution. (a): 10km for the first three cycles, starting at 00 UT on Days 1, 2, and 3, respectively. Red arrows show the transfer of initial conditions to both the next day's 10km forecast cycle and the 2.5km forecast (the latter also makes use of hourly 10km output values as lateral boundary conditions). (b): 2.5km forecasts for the first three cycles, starting at 00 UT on Days 1, 2, and 3, respectively. Blue arrows are used to show the transfer of 24 hours of hour-ending 2.5km output to the timeline of model output used for evaluation. (c): Resulting record of successive 24 hour 2.5km grid cell size GEM-MACH forecasts, created by combining the hour-ending values between 04 UT on day N through to 03 UT on day N+1.

As shown in Figure S.1, both model resolutions employ a 27-hour cycle starting at 00 UTC each day, with both the 10 km and 2.5 km simulation receiving chemical tracer initial conditions from the previous day's 10km simulation. Meteorological boundary conditions for the 10 km simulation (Figure S.1a) are from the *a priori* GEM forecasts employing data assimilated meteorological analysis input fields as noted above. Chemical boundary conditions for most species for the 10 km simulation (Figure S.1a) are taken from the average of a 2009 MOZART global simulation and analysis (Emmons *et al*., 2010), and the 10 km simulation boundary concentration of benzene and PAHs are assumed to be zero. The 27 hour, 10 km resolution GEM-MACH simulations in turn provide chemical and meteorological chemical initial and boundary conditions for each cycle's 2.5km domain simulation (Figure S.1b). The first 3 hours (hours ending 01, 02 and 03 UT) of the 2.5 km simulation are treated as meteorological spin-up, to allow the high-resolution cloud microphysics to approach a quasi-steady-state. These first three hours are discarded, and the final 24 hours (hours 04 UT on day N to 03 UT on day N+1) are retained (Figure S.1c). The resulting set of daily 2.5 km forecast simulations (from 4 UT on day N to 3UT on day N+1) are stitched together to create a contiguous series of model outputs (Figure S.1c). The continuity between forecasts is preserved at the 10 km level, with the 00 UT concentrations of the forecast starting on day N being used to initialize the forecast of day N+1. This strategy was employed in order to make maximum use of the meteorological analysis fields (available at 10 km resolution), and allow spin-up time for the hydrometeor representation in the 2.5 km resolution simulation, while employing the better spatial representation of PAH concentrations and chemistry resulting from

the 2.5 km resolution GEM-MACH-PAH simulations. We run this cycling setup for the spring-summer and fall-winter time periods mentioned in the main paper, each with a 1-week spin up for the air concentrations fields to stabilize.

The modelled mixing ratios from the 2.5 km simulations were output in units of $\mu g\ kg^{-1}$ with aerosols sectioned into two size bins based on aerodynamic diameter (fine fraction= 0–2.5 $\mu m$ and coarse fraction = 2.5-10 $\mu m$). Results presented herein were converted to volumetric concentrations ($\mu g\ m^{-3}$ and $ng\ m^{-3}$ for BENZ and PAH, respectively) and PAH concentrations were summed across the gas and particle phases to yield total concentrations.

### *Improvements to Simulated Spatial Variability Relative to Previous Work*

PAH measurements from NAPS in Hamilton, Ontario, Canada, were used in a previous evaluation of an earlier 42-km resolution PAH model (Galarneau *et al*, 2014), and varied from 52-117% depending on the PAH species (coefficient of variation of measurements within the 42-km Hamilton model grid square), suggesting that the latter model resolution was not adequate for the study of areas with steep concentration gradients such as cities. Shrinking the grid size from 42 km to 2.5 km in the current study reduced average coefficients of variation to 19-41% when assessed using more recent measurements (Anastasopoulos *et al*, 2012), demonstrating that higher resolution improves model representativeness within urban areas. Observed variability within the area covered by some of the Hamilton 2.5 km grid squares reached values as high as 80%, however, thus modelled concentration variability across urban areas or near otherwise isolated industrial sources may still be underestimated. The latter sub-grid variability combined with uncertainties associated with the spatial allocation of mobile source emissions (see Emissions section of the main paper) complicate the interpretation of model results at the intra-urban scale. However, our results are in accord with previous air quality model simulations of organic aerosol and ozone formation for this region (Stroud *et al*, 2011; Makar *et al*., 2010), which show that 2.5 km resolution is necessary to adequately resolve the chemistry-meteorology interactions associated with lake-breeze circulation.

### *Fall-Winter Results for BENZ and BaP*

The fall-winter BENZ emissions data available for the study did not include residential wood combustion (RWC) due to inventory processing issues. Since the latter source is non-negligible for BENZ in fall-winter (vs. spring-summer when RWC emissions are small), the contribution of on-road mobile sources is skewed by its omission and therefore fall-winter BENZ has not been reported here. PAHs and all other criteria contaminants from RWC were included in the emissions used in this study. In addition, the positive bias in modelled BaP concentrations noted above for the "base" case during fall-winter precludes the use of this version of the model for the determination of BaP source contributions for this season.

## II.    Fall-winter average maps of PHEN and PYR

Figure S.2 below shows the fall-winter averages of PHEN and PYR modelled concentrations, as well as absolute and relative on-road vehicle contributions, consistent with Figures 2-4 in the main paper, which are for the same, respectively, but in the spring-summer.
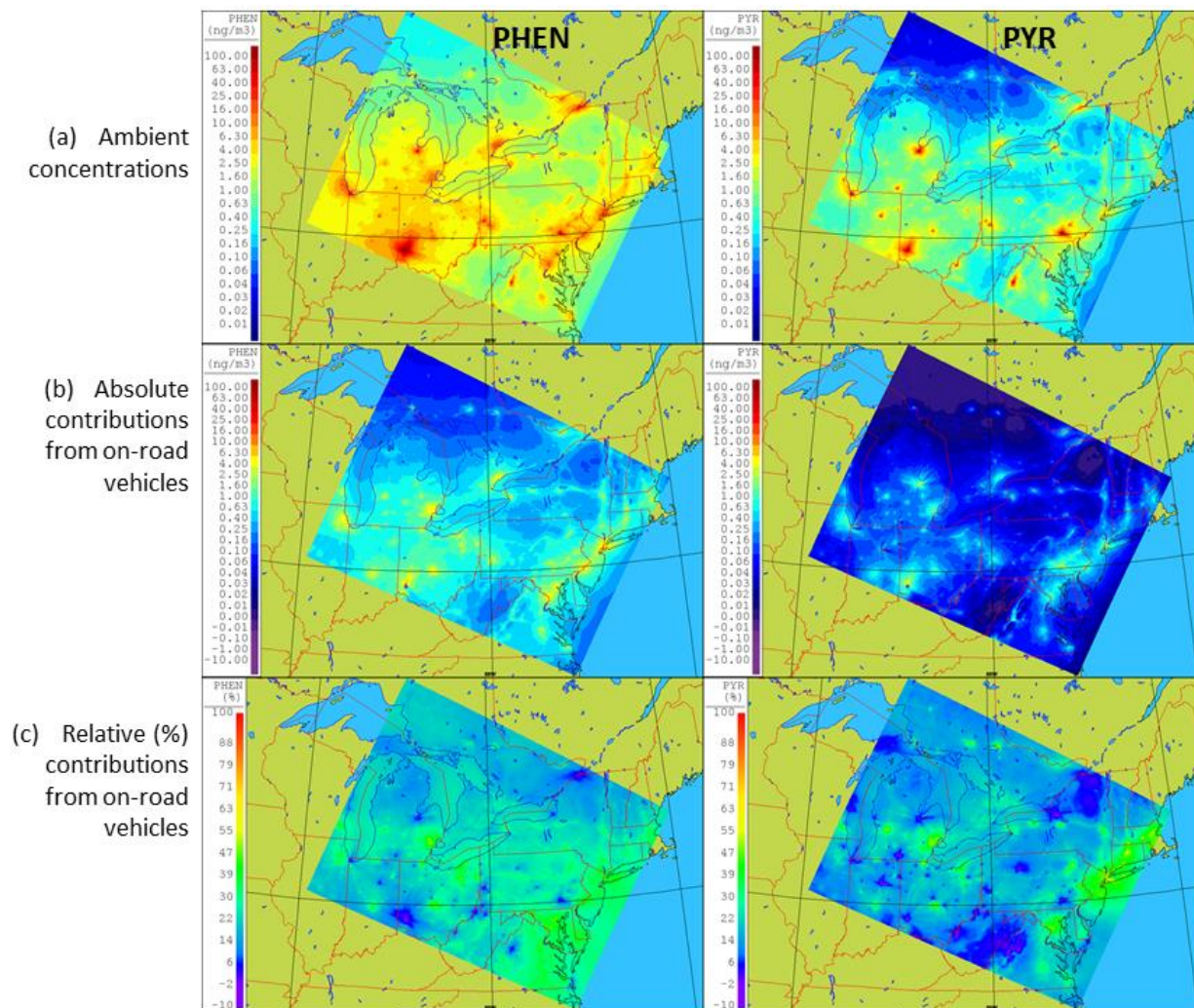
**Figure S.2:** Fall-winter average maps for PHEN and PYR (a, b, and c are extensions of Figures 2, 4, and 5 in the main paper, respectively).

### III. BENZ and PAH emissions in the model domain

Figure S.3, as discussed in the main paper, shows the BENZ and PAH domain and seasonal-average emissions used as input to GEM-MACH-PAH.
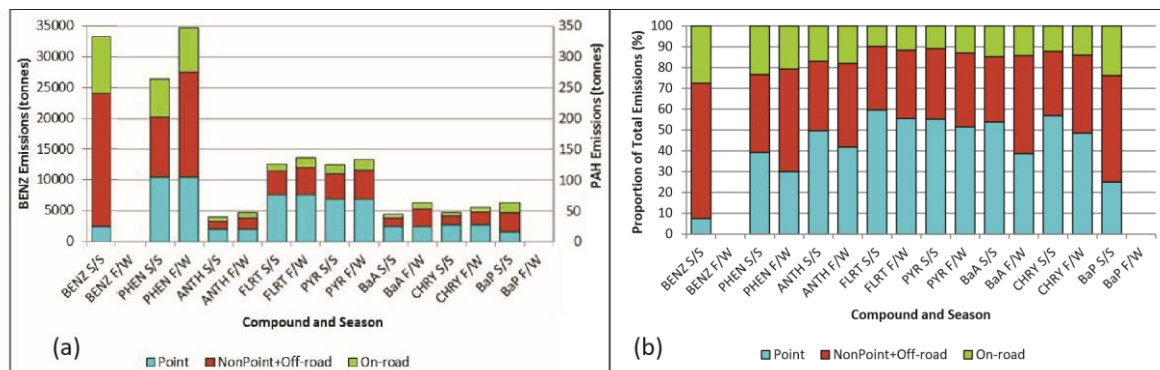
**Figure S.3:** Total (a) and fractional (b) high-resolution domain-wide emissions in spring-summer and fall-winter.

### IV. Absolute on-road vehicle contributions in selected cities in spring-summer 2009.

Figure S.4 depicts the absolute mobile contributions to ambient concentrations of benzene and pyrene in selected cities in the domain, and suggests that the spatial distribution of on-road vehicle contributions differs between urban areas in Canada and the US, with the U.S. model output showing higher mobile contributions at the centre of cities, and Canada's having higher mobile contributions along the major highways, and relatively little at the city centres. This difference is due to differences in (a) the available Canadian and US national emissions inventories, and (b) the resulting subsequent emissions processing practices employed in the two different jurisdictions. All on-road vehicle emissions in Canada are reported by road type and are then spatially allocated from provincial totals to road and highway networks using SMOKE. In contrast, about 60% of US on-road vehicle VOC emissions estimated using MOVES 2010b are categorized as "off-network" and are allocated to locations such as parking lots and driveways, following a population spatial surrogate. The differences created by the two inventory breakdowns and spatial allocation approaches can be seen in this figure. In Toronto (left-most maps), on-road vehicle concentration maxima occur along major highways in the region with the effect of distributing pollutant mass toward suburban areas. In American cities (right 3 columns), the mobile source maxima are more narrowly concentrated in urban cores. As a result of this difference in emission allocation, itself resulting from the inventory data and processing used in each country, cross-border differences in intra-urban spatial distribution of modelled concentrations and on-road vehicle contributions should be interpreted with caution.
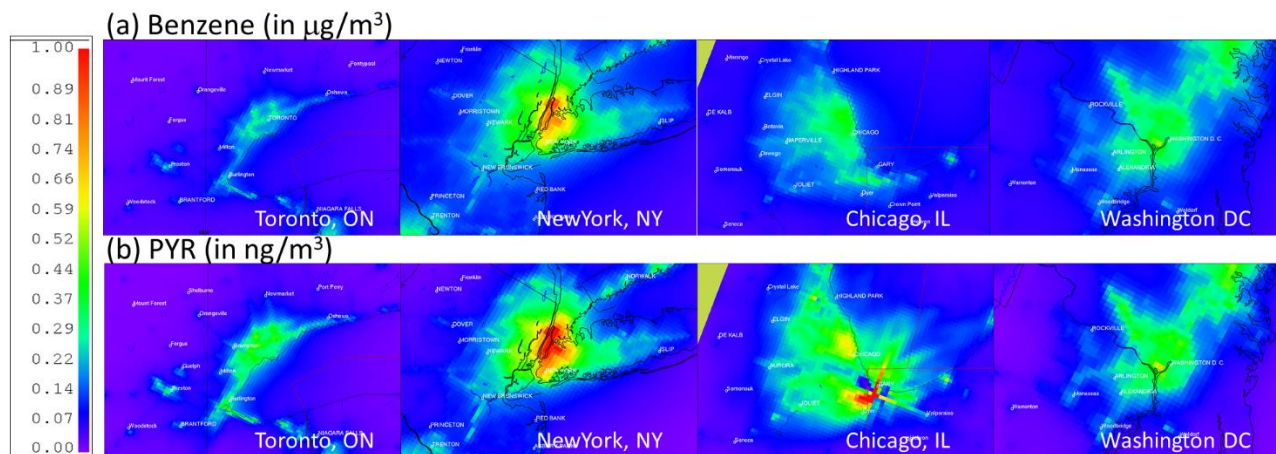
**Figure S.4:** Spring-summer seasonal average absolute contributions of on-road vehicles to (a) BENZ, and (b) PYR ambient concentrations in four large metropoles in the model domain. Note the colour scale is linear and benzene is in μg m⁻³, whereas PYR is in ng m⁻³.

### V.      Sensitivity Considerations

*Sensitivity to the variability in vehicle emission factors*
As noted in the manuscript, four simulations were conducted to assess the sensitivity of model results to the variability in emission factors reported in the published literature. The simulations used on-road vehicle benzene and PAH emissions that were scaled by factors of 0.5 and 2 in accordance with the 25th and 75th percentile range of emission factors found in the recent literature (Whaley *et al*., 2018), whereas vehicle emissions of other compounds (e.g., volatile organic compounds, primary particulate matter, etc.) were unchanged. The simulations were run for two weeks each in the spring and fall periods. These sensitivity simulations show the range of vehicle contributions to ambient concentrations that would be encountered if vehicle emission factors varied away from the MOVES 2014 values that were used in the "base" case (while holding all other quantities constant). We note again that initial model testing yielded better simulation quality when compared to available measurements for emission factors from MOVES2014 than from the recently-published literature, yet the range of reported factors is large and therefore worthy of examination.

Table 2 in the main paper summarizes the results of these sensitivity simulations. When compared to the base case results shown in the "average" rows of Table 1, the modelled system is shown to respond predictably to changes in the emissions inputs from mobile sources. Halved vehicle emissions reduce mobile source emissions contributions to concentrations from 4-21% and 14-24% in spring-summer and fall-winter, respectively, to 0.5-11% and 4-12%. Similarly, doubled emissions increase mobile source contributions to concentrations to 4-42% and 27-41%.  These results show that the modelled domain-wide seasonal averages respond consistently (and nearly linearly) to changes in on-road vehicle emissions for BENZ and PAHs.

*Sensitivity to oxidants*
Further insights into the sensitivities of the model system can be obtained by examining responses observed when a class of emissions is removed for all emitted species, such as in the study's "no mobile" scenario. Changes in BENZ and PAH concentrations under such a scenario arise from two factors: (1) changes to emissions themselves, and (2) changes to the overall lifetimes of remaining (non-vehicle) BENZ and PAH. Whereas the first factor is straightforward to manipulate as shown in the sensitivity tests described above, the second factor is complex to assess because it arises largely as a result of secondary formation processes for atmospheric oxidants such as hydroxyl radical and ozone. A cut in emissions does not necessarily yield a linear change in oxidant concentrations, but rather a range of changes that rely not only on chemistry but on the physical state of the atmosphere at each location. The range of responses in BENZ and PAH concentrations as a function of changes in oxidant concentrations is described below, and then compared to a similar analysis relative to emissions changes.

Figure S.5 below shows the absolute change in seasonal-average surface concentrations of pyrene as a function of changes in OH in each model grid square due to on-road vehicle emissions.
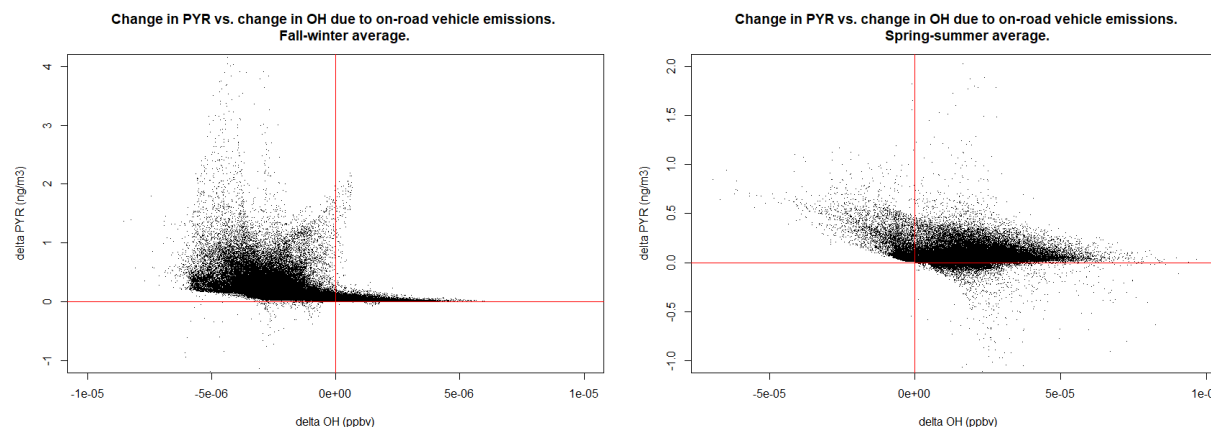
**Figure S.5:** Change in seasonal-average surface pyrene concentrations vs OH concentrations due to on-road vehicle emissions (delta=[base – nomobile]). (left) fall-winter (right) spring-summer. Note change in axis scales between the two figures.

In the fall-winter (Fig. S.5, left), on-road vehicle emissions are associated with lower OH concentrations than those predicted from total base case emissions. This is predicted for 77% of the model domain ($\Delta$OH < 0 along x-axis of Fig S.5; see also top right panel of Fig S.5), and is consistent with known $NO_x$-VOC-$O_3$ chemistry:

 (1) On-road vehicle emissions contribute $NO_x$ to the atmosphere,

 (2) In the low-temperature, low-light conditions of winter, this additional $NO_x$ drives down concentrations of $O_3$ over the entire region (e.g., Fig S.4, 2$^{nd}$ row, right) in titration reactions.

 (3) The decrease in $O_3$ leads to a decrease in OH concentrations, via the reactions:

$$O_3 + h\nu \rightarrow \alpha\, O^{(1D)} + (1-\alpha)\, O^{(3P)} + O_2$$
$$O^{(1D)} + H_2O \rightarrow 2\, OH$$
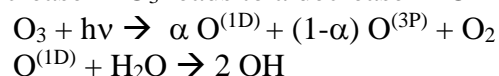
For a smaller number of grid squares (23%; Fig S.5, top-right), on-road vehicles contribute to higher OH concentrations than those predicted from total base case emissions ($\Delta$OH > 0 along x-axis of Fig S.5), with the resulting potential to transform more pyrene via oxidation. However, $\Delta$pyrene remains positive in 99.9% of the domain, demonstrating that the net impact of increased oxidation reactions is secondary to that of the emissions.

Thus, this analysis shows that removing on-road vehicle emissions in fall-winter will decrease pyrene in two ways. First directly, through the reduction in pyrene mass due to the emissions themselves, and next indirectly, via increased OH oxidation resulting from higher $O_3$ levels (in turn the result of reductions in $NO_x$ titration).

The spring-summer relationship between on-road vehicle emissions and chemistry is more complex. While the $NO_x$ titration regime is still *present* on the negative side of the $\Delta$OH axis (at only 4% of the points, which are seen in major cities in Fig S.5, top left, likely corresponding to the impact of nighttime titration of $O_3$ by vehicle $NO_x$ emissions), the vast majority of points appearing on the positive side of the $\Delta$OH axis (Figure S.6, right, and in Fig S.5, top left) correspond to increased photochemical production of $O_3$ caused by on-road vehicle emissions. The latter situation arises as the less stable, higher photolysis environment of summer daytime conditions, along with increased $NO_x$ and VOC emissions from on-road vehicles, lead to increased OH concentrations. However, once again, the change in pyrene is nearly always positive (88%):

the reduction in pyrene concentrations associated with removing mobile emissions nearly always dominates, despite changes in the oxidative environment. The effect of oxidation on pyrene concentrations is thus shown to be a secondary effect compared to the emissions reductions themselves.

A key result of this analysis is that in both spring-summer and fall-winter cases, the changes in pyrene mobile emissions are the dominating factor controlling pyrene concentrations at most locations, and that average pyrene concentrations are expected to decrease if emission from on-road vehicles are removed. However, some locations are subject to unexpected changes in PAH concentrations due to the interplay of factors that control atmospheric oxidants. This finding demonstrates that there is added value in using an atmospheric model to determine the effect of emission contributions on atmospheric concentrations beyond what can be learned by examining emission changes alone.

Particulate BaP has an on-particle reaction with $O_3$ in the model, and Figure S.6 shows a scatterplot for changes in BaP relative to changes in $O_3$. As discussed in the paper, and as shown in Figure S.5, on-road vehicle emissions contribute to increased $O_3$ across most of the domain. Some areas are associated with BaP decreases (negative $\Delta$BaP values) due to vehicle emissions (Figures 3d & 4d in the main manuscript). At those locations, BaP degradation associated with the increased $O_3$ (and OH) is larger than the the BaP contributed by the on-road vehicle emissions, leading to a net *decrease* in BaP. However, 98.9% of locations are predicted to have positive contributions of BaP from vehicle emissions despite changes in oxidation conditions. Similar to the examples above for pyrene and phenanthrene, this analysis demonstrates that the role of atmospheric oxidants is secondary to changes in emissions at the majority of locations in the study domain.
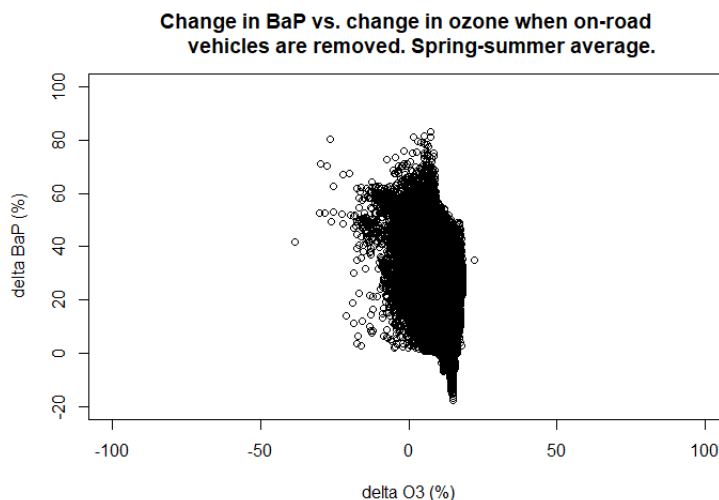
**Figure S.6:** Change in spring-summer average surface benzo(a)pyrene concentrations vs ozone concentrations due to on-road vehicle emissions. All changes in concentration are period averages for (base) – (no mobile emissions), expressed as a percent of the base scenario at each grid square.

*Sensitivity to vehicle emissions*
At the beginning of this section, we reported on direct sensitivity tests to examine the effect of uncertainty in on-road vehicle emissions on simulated BENZ and PAH concentrations. We then examined the range of oxidant chemistry effects using scatterplot analyses of on-road vehicle

contributions to various parameters. As a final examination of sensitivity, we apply the scatterplot approach used above for oxidants to the analysis of emissions contributions from vehicles in order to compare results using a common methodology. In Figure S.7 below, we show the absolute change to PYR concentrations ("base" – "no mobile") as a function of on-road vehicle emissions in the same grid cell for both time periods studied. The absolute change to PYR concentration shows substantial scatter where vehicle emissions are small, and decreasing variability as the magnitude of those emissions increases. This further supports our previous analysis demonstrating that the effect of emissions predominates relative to oxidant chemistry in most of this highly populated model domain. The oxidant chemistry only has a comparable influence on PAH concentrations as do emissions changes where on-road vehicle emissions are relatively small.
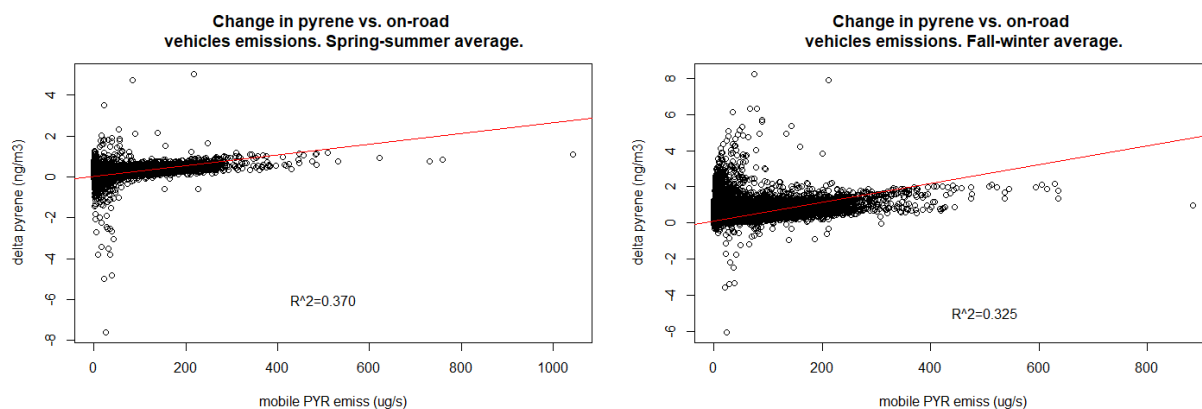
**Figure S.7:** Seasonal average absolute change in pyrene concentration as a function of seasonal average on-road vehicle emissions of pyrene at each grid square.

## VI.     Relative (percent) on-road vehicle contributions (additional PAHs).

Table 1 and Figures 4 (in main paper), S.2c and S.8 all show the relative contribution of on-road vehicles as a percent of total benzene and PAH concentrations. Table 1 reports on domain-wide seasonal averages, whereas Figures 4, S.2c, and S.8 shows how the seasonal averages vary over space.
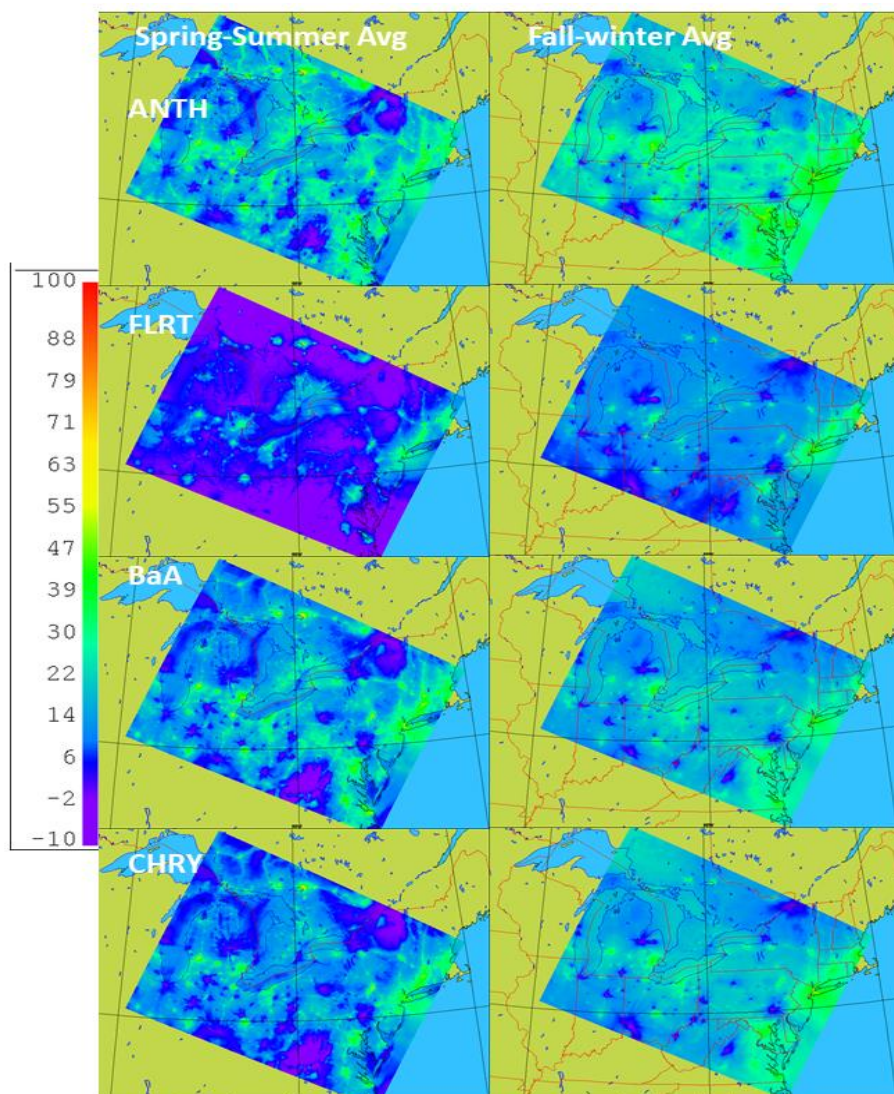
**Figure S.8:** Relative (percent) contributions of on-road vehicles to ambient concentrations of ANTH, FLRT, BaA, and CHRY. Left column for spring-summer, right column for fall-winter.

## VII. Relative (percent) on-road vehicle contributions to oxidants, particulate matter (PM₁₀) and elemental carbon (EC₁₀).

Figure S.9 shows the seasonal average on-road vehicle contributions to oxidants and particulate matter. When the "contribution" is negative, this means that the removal of vehicle emissions would cause an increase in that species.
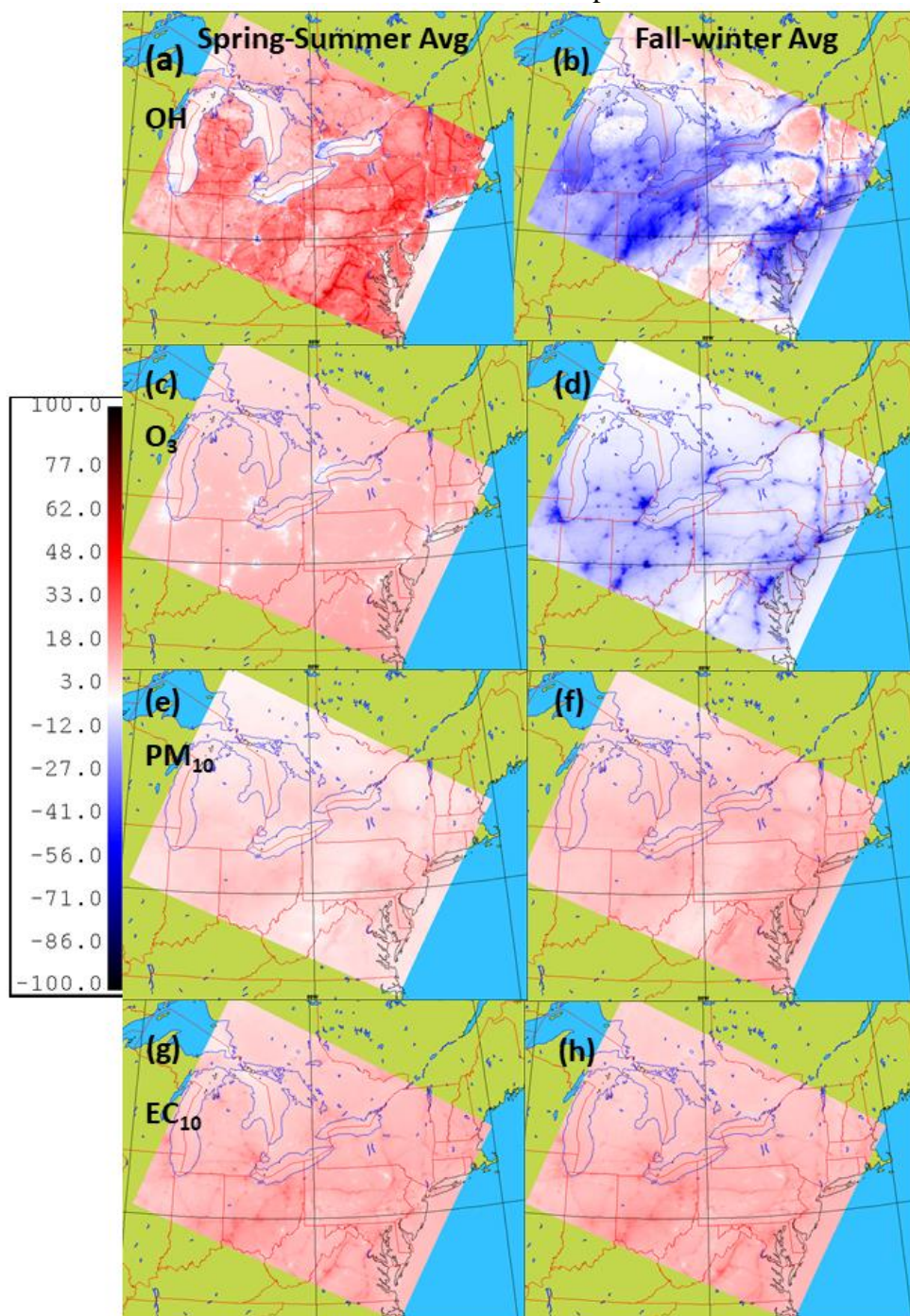
**Figure S.9:** Relative (percent) change in ambient concentrations of OH, $O_3$, $PM_{10}$ and $EC_{10}$. Left column for spring-summer, right column for fall-winter.

**References:**

Dachs, J. and Eisenreich, S. J.: Adsorption onto aerosol soot carbon dominates gas-particle partitioning of polycyclic aromatic hydrocarbons, Environ. Sci. Technol., 34, 3690–3697, https://doi.org/10.1021/es991201, 2000.

Franz, T. P. and Eisenreich, S. J.: Snow scavenging of polychlorinated biphenyls and polycyclic aromatic hydrocarbons in Minnesota, Environ. Sci. Technol., 32, 1771–1778, https://doi.org/10.1021/es970601z, 1998

Galarneau, E., Makar, P. A., Zheng, Q., Narayan, J., Zhang, J., Moran, M. D., Bari, M. A., Pathela, S., Chen, A., and Chlumsky, R.: PAH concentrations simulated with the AURAMS-PAH chemical transport model over Canada and the USA, Atmos. Chem. Phys., 14, 4065–4077, https://doi.org/10.5194/acp-14-4065-2014, 2014.

Kwamena, N.-O., Thornton, J. A., and Abbatt, J. P. D.: Kinetics of surface-bound benzo(a)pyrene and ozone on solid organic and salt aerosols, J. Phys. Chem., 108, 11626–11634, https://doi.org/10.1021/jp046161x, 2004.

Makar, P.A., Zhang, J., Gong, W., Stroud, C., Sills, D., Hayden, K.L., Brook, J., Levy, I., Mihele, C., Moran, M.D., Tarasick, D.W., He, H., and Plummer, D., Mass tracking for chemical analysis: the causes of ozone formation in southern Ontario during BAQS-Met 2007, Atmos. Chem. Phys. 10, 11151-11173, 2010.

Makar, P.A., Akingunola, A., Aherne, J., Cole, A.S., Aklilu, Y-A., Zhang, J., Wong, I., Hayden, K., Li, S.-M., Kirk, J., Scott, K., Moran., M.D., Robichaud, A., Cathcart, H., Baratzedah, P., Pabla, B., Cheung, P., Zheng, Q., Jeffries, D.S., Estimates of exceedances of critical loads for acidifying deposition in Alberta and Saskatchewan, Atmos. Chem. Phys., 18, 9897-9927, 2018.

SAPRC-07, W. P. L. Carter: Development of the SAPRC-07 Chemical Mechanism, Atmospheric Environment, 44, 5324-5335, 2010.

Stroud, C.A., Makar, P.A., Moran, M.D., Gong, W., Gong, S., Zhang , J., Hayden, K., Mihele, C., Brook, J.R., Abbatt, J.P.D., and Slowik, J.G, Impact of model grid spacing on regional- and urban-scale air quality predictions of organic aerosol, Atmospheric Chemistry and Physics, 11, 3107-3118, 2011.

Whaley, C.H., Galarneau, E., Makar, P.A., Akingunola, A., Gong, W., Gravel, S., Moran, M.D., Stroud, C., Zhang, J., Zheng, Q., GEM-MACH-PAH (rev2488): a new high-resolution chemical transport model for North American polycyclic aromatic hydrocarbons and benzene, Geosci. Model Dev., 11, 2609-2632, https://doi.org/10.5194/gmd-11-2609-2018, 2018.